Using L-Arginine-Functionalized Gold Nanorods for Visible Detection of Mercury(II) Ions

Jiehao Guan, Yi-Cheng Wang, and Sundaram Gunasekaran

Abstract: A rapid and simple approach for visible determination of mercury ions (Hg^{2+}) in aqueous solutions was developed based on surface plasmon resonance phenomenon using L-arginine-functionalized gold nanorods (AuNRs). At pH greater than 9, the deprotonated amine group of L-arginine on the AuNRs bound with Hg^{2+} leading to the side-by-side assembly of AuNRs, which was verified by transmission electron microscopy images. Thus, when Hg^{2+} was present in the test solution, a blue shift of the typical longitudinal plasmon band of the AuNRs was observed in the ultra violet-visible-near infrared (UV-Vis-NIR) spectra, along with a change in the color of the solution, which occurred within 5 min. After carefully optimizing the potential factors affecting the performance, the L-arginine/AuNRs sensing system was found to be highly sensitive to Hg^{2+}, with the limit of detection of 5 nM (S/N = 3); it is also very selective and free of interference from 10 other metal ions (Ba^{2+}, Ca^{2+}, Cd^{2+}, Co^{2+}, Cs^{+}, Cu^{2+}, K^{+}, Li^{+}, Ni^{2+}, Pb^{2+}). The result suggests that the L-arginine-functionalized AuNRs can potentially serve as a rapid, sensitive, and easy-to-use colorimetric biosensor useful for determining Hg^{2+} in food and environmental samples.

Keywords: colorimetric sensor, food safety, green synthesis, heavy metal, surface plasmon resonance, water quality

Practical Application: In this paper we present a rapid, sensitive, and easy-to-use method for detecting amount of mercury ions present in water. Using L-arginine-functionalized gold nanorods, which change in color when mercury is present in the sample, we are able to detect as low as 5 nM of mercury within 5 min. This method can be useful for routine measurement of mercury present in food and environmental samples

Introduction

Mercury is one of the most toxic elements that have adverse effects on humans and biological system (Tchounwou and others 2003; Selin 2009), and the water-soluble mercury(II) ion (Hg^{2+}) is one of the most common forms of mercury pollution. Mercury tends to be bioaccumulated and biomagnified in aquatic food chains (Clarkson and others 2003; Leopold and others 2010). Consequently, consumption of fish and other seafood is one of the most important exposure routes for mercury (Al-Mughairi and others 2013; Greenfield and others 2013). Based on the Natl. Health and Nutrition Examination Survey, mercury levels were 4-fold higher in people who ate 3 or more servings of fish per month than in those who did not consume seafood (Schober and others 2003). Since fish contain higher levels of mercury that may harm an unborn baby or young child's developing nervous system, the U.S. Food and Drug Administration and Environmental Protection Agency have advised that pregnant women, nursing mothers, and young children completely avoid certain fish and other seafood (especially shark, swordfish, king mackerel, and tilefish) that contain significantly high levels of mercury (FDA 2014). Mercury exposure can also damage a variety of human organs, such as kidney and brain and compromise immune, nervous, and endocrine systems (Clarkson and others 2003; Nolan and Lippard 2008; de Souza and de Carvalho 2009; Mutter and others 2010; Mamdani and Vettese 2013).

MS 20141537 Submitted 9/14/2014, Accepted 12/23/2014. *Authors are with Dept. of Biological Systems Engineering, Univ. of Wisconsin-Madison, 460 Henry Mall, Madison, WI, U.S.A. Direct inquiries to author Gunasekaran (E-mail: guna@wisc.edu).*

The determination of mercury ions in contaminated samples is generally performed by instrumental methods, such as inductively coupled plasma mass spectrometry (Ugo and others 2001), high-performance liquid chromatography (Balarama Krishna and others 2007), atomic absorption spectrometry (Hsu and others 2011), and electrochemical methods (Zhu and others 2009). Although these methods offer excellent sensitivity, their major drawbacks are high cost and complex and time-consuming test protocols. Hence, the development of a simple, rapid, economical, and sensitive method for mercury detection is needed for detecting mercury ions in food and environmental samples (Male and others 2013; Mansour 2014; Yasri and others 2014).

Colorimetric sensors are convenient and attractive because they allow prompt monitoring without the need for read-out devices or trained personnel to perform the test (Nolan and Lippard 2008; Lim and others 2012). Much research has been done on designing optical sensing systems for detecting mercury ions based on conjugated polymers (Qu and others 2014), biomolecules, such as proteins (Guo and others 2011), DNA (Xue and others 2008; Wei and others 2014), oligonucleotide (Liu and others 2007), and quantum dots (Li and others 2011; Chen and others 2014), and inorganic materials (Tao and others 2014). Moreover, functionalized gold nanoparticles (AuNPs) have been widely used in biosensors due to the distinct surface plasmon resonance properties (Jans and Huo 2012; Wang and Gunasekaran 2012; Hutter and Maysinger 2013; Wang and others 2015), including for the detection of heavy metals, such as Hg^{2+}, Pb^{2+}, Cu^{2+} (Lin and others 2011; Chen and others 2014). Compared to AuNPs, which are typically spherical and exhibit 1 plasmon band at around 520 nm, anisotropic nanoparticles such as nanorods exhibit 2 plasmon bands, owing to the oscillation of electrons along transversal

doi: 10.1111/1750-3841.12811

Journal of Food Science A Publication of the Institute of Food Technologists

and longitudinal directions. The transversal peak of gold nanorods (AuNRs) remains at around 500 nm, however, their longitudinal plasmon band is located anywhere in the visible to near infrared range (600 to 900 nm), depending on their aspect ratio (Jana and others 2001). Interestingly, the longitudinal plasmon band of AuNRs has a higher extinction coefficient, rendering AuNRs more sensitive to changes in the dielectric properties of the surrounding environment, which could improve the performance of biosensors (Vigderman and others 2012; Placido and others 2013). Herein, we describe a green method using L-arginine, one of the proteinogenic amino acids, to modify AuNRs and use this green-functionalized AuNRs for visible detection of Hg^{2+} in water. The possible mechanism for this visible detection system and its sensitivity, selectivity, limit of detection (LOD) of Hg^{2+} are also discussed.

Materials and Methods

Materials

Hydrogen tetrachloroaurate (III) trihydrate ($HAuCl_4 \cdot 3H_2O$), sodium borohydride ($NaBH_4$, ≥98%), silver nitrate ($AgNO_3$, 99.85%) were from Acros Organics (Morris Plains, NJ, USA). Cetyltrimethyl ammonium bromide (CTAB) was from MP Biomedicals (Solon, OH, USA). L-ascorbic acid (AA, ≥99%) and sodium hydroxide (NaOH) were from Fisher Scientific.

For heavy metals, Mercury(II) nitrate monohydrate ($Hg(NO_3)_2.H_2O$, ≥98%), lead(II) chloride ($PbCl_2$, 99%), nickel(II) chloride hexahydrate, ($NiCl_2 \cdot 6H_2O$, 97%), zinc chloride, ($ZnCl_2$, 97%), lithium chloride, (LiCl, ≥99%) were from Acros Organics. Cupric chloride, dihydrate, ($CuCl_2 \cdot 2H_2O$, 99%) was from Sigma-Aldrich (St. Louis, MO). Calcium chloride

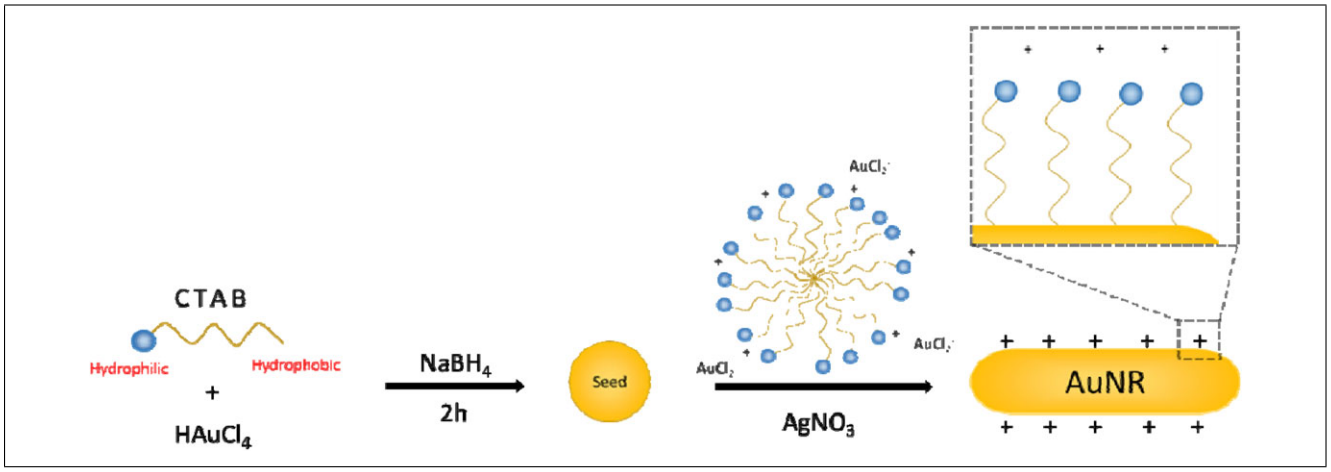

Figure 1–Scheme for seed-mediated method for synthesis of gold nanorods (AuNRs). The seed is first prepared by mixing cetyltrimethyl ammonium bromide (CTAB) with $HAuCl_4$, followed by adding $NaBH_4$ and kept at 29 °C for 2 h. Then, the seed solution is added to the growth solution, which includes $HAuCl_4$, CTAB, HCl, and $AgNO_3$ and L-ascorbic acid, and kept at 29 °C overnight to complete the synthesis of AuNRs.

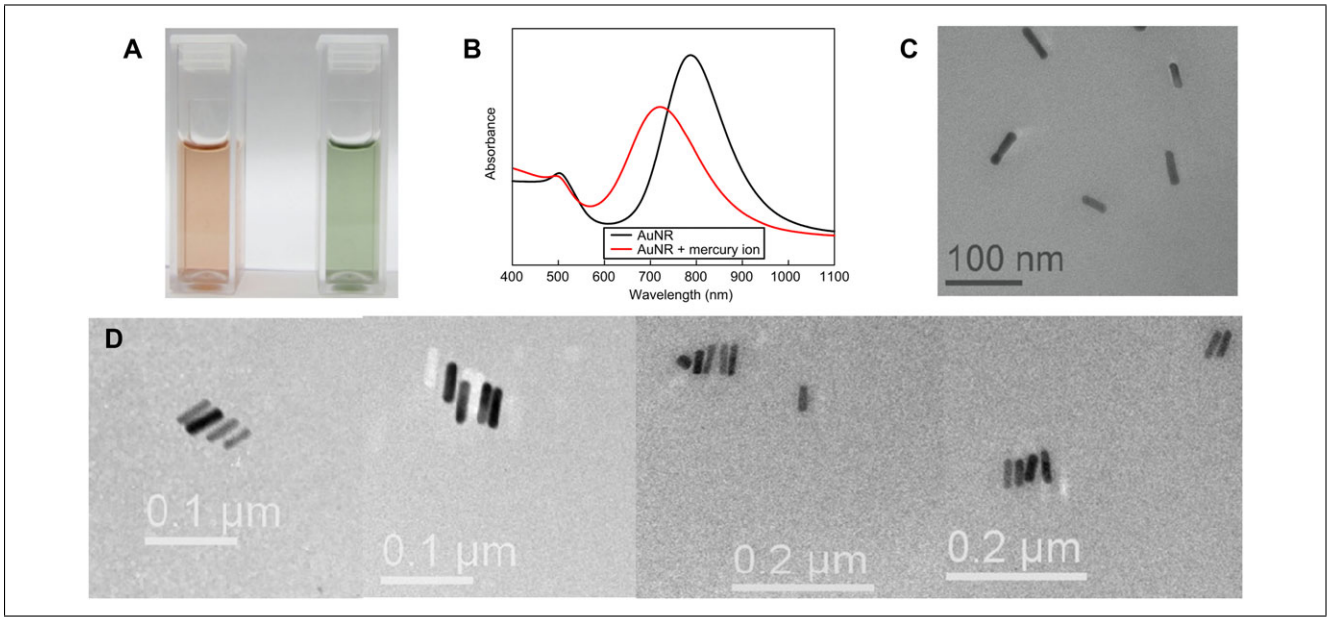

Figure 2–Effect of adding 1 mM Hg^{2+} to L-arginine-functionalized gold nanorods (AuNRs) solution: color (a) before (left) and after (right) Hg^{2+} addition; absorption spectra (b); and TEM micrographs before (c) and after (d) Hg^{2+} addition.

dihydrate ($CaCl_2 \cdot 2H_2O$, ≥99%), barium dichloride dihydrate ($BaCl_2 \cdot 2H_2O$, 100% w/v), potassium chloride (KCl, ≥99%), from Fisher Scientific (Rockford, IL). Cobalt chloride hexahydrate ($CoCl_2 \cdot 6H_2O$, ≥99%) and cadmium chloride ($CdCl_2$, ≥99%) were purchased from MP Biomedicals. These chemicals were used as received without any purification. All aqueous solutions were prepared in deionized water of resistivity ≥18.2 MΩ·cm (Ultrapure water system, Millipore, (Billerica, MA)).

Equipment

Absorption spectra (400 to 1100 nm) were recorded using Lambda 25 UV-Vis-NIR spectrophotometer (PerkinElmer (Perkin Elmer, MA)). Morphology of AuNRs was determined using FEI (Hillsboro, OR) Tecnai T12 transmission electron microscope (TEM) operating at 120 kV. Typically, samples were prepared by dropping the solution on a carbon-coated 400 mesh copper grid and excess solution was removed by wicking with filter paper. The grid was allowed to dry at room temperature before imaging.

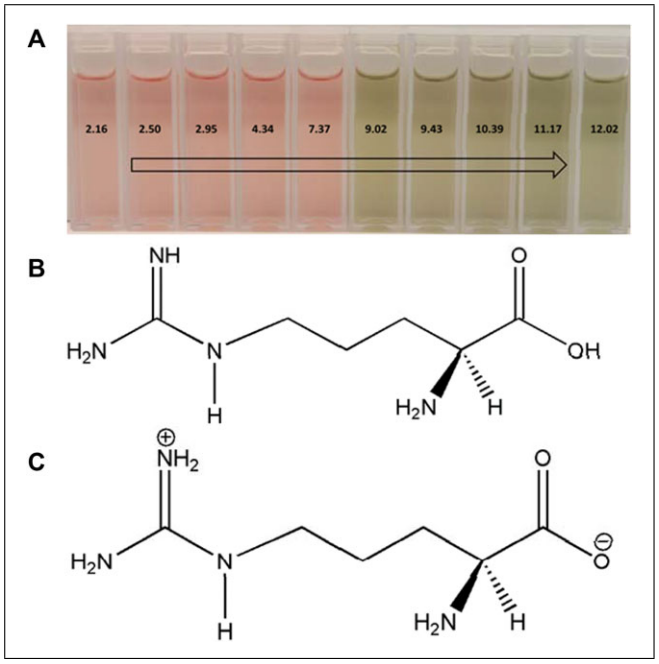

Figure 3–(a) Color of L-arginine-functionalized gold nanorods solution with 1 mM Hg^{2+} at different pHs. The pH of solution is controlled by adding different amount of 0.1 M NaOH. (b) Chemical structure of L-arginine, and (c) structure of L-arginine at pH higher than 9 (pKa_2) but lower than 12.48 (pKa_3).

Synthesis and L-arginine functionalization of AuNRs

AuNRs were synthesized following a published seed-mediated protocol with slight modification (Orendorff and Murphy 2006). Figure 1 shows the scheme for synthesis of AuNRs. Briefly, a seed solution is first prepared by reducing 250 μL 10 mM $HAuCl_4$ in 9.75 mL 0.1 M CTAB with 800 μL ice-cold 0.01 M $NaBH_4$ under vigorous stirring for 1 min and placing in water bath at 29 °C for 2 h. A yellow to brownish-yellow color change of the solution signifies the formation of gold seeds.

The growth solution was prepared by adding 1 mL 10 mM $HAuCl_4$ into 40 mL of 0.1 M CTAB with gentle mixing, followed by 40 μL of 0.1 M $AgNO_3$ and 800 μL of 1 M HCl, and finally 160 μL of 0.1 M L-AA. The color of the solution eventually changes from dark yellow to being colorless. For synthesizing AuNRs, 160 μL of the seed solution was added into the growth solution and kept overnight in a water bath at 29 °C. The samples were characterized by UV-Vis-NIR spectroscopy and TEM.

For L-arginine functionalization, 1 mL of the AuNRs solution was gently mixed with 1 mL 0.5 mg/mL L-arginine. After 5 min, the pH of the mixed solution was adjusted by successive addition of 0.1 M HCl/NaOH to determine the optimal pH. The resulting solution was incubated for 5 min at room temperature and its absorption spectrum was recorded. The morphology of AuNRs was determined by TEM.

Determination of Hg^{2+}

To determine the Hg^{2+} content in water, 1 mL of different known concentrations of Hg^{2+} were added into the L-arginine/AuNRs solution and incubated at room temperature for 5 min. The observed color and absorption spectra of the solution were recorded and the morphology of AuNRs were determined by TEM. To evaluate the specificity of Hg^{2+} detection, 10 mM solution of different metal ions, such as Ba^{2+}, Ca^{2+}, Cd^{2+}, Co^{2+},

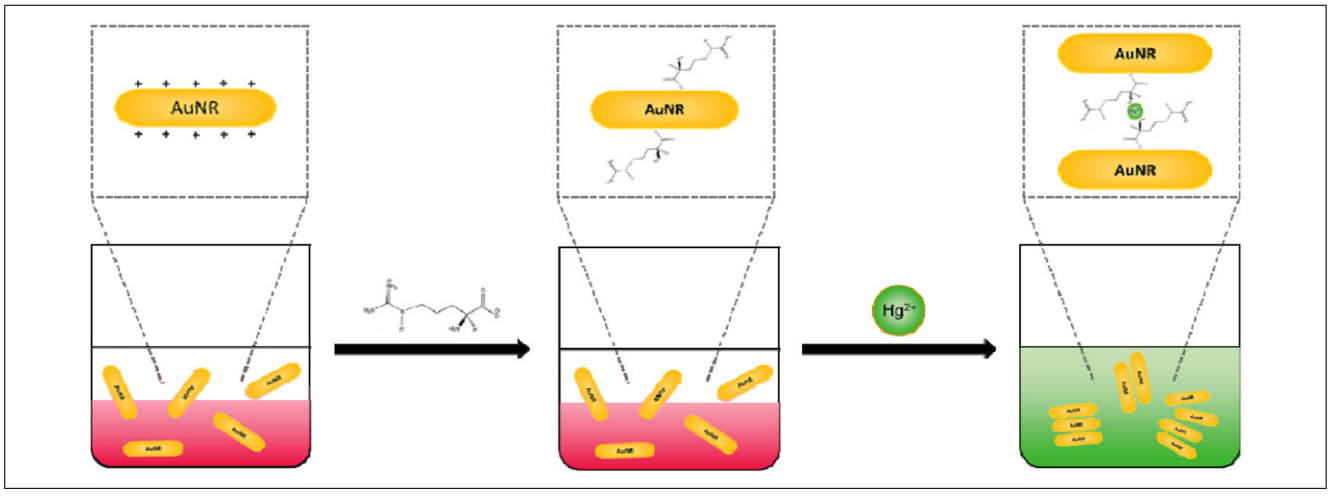

Figure 4–Mechanism of using L-arginine-functionalized AuNRs for visible detection of Hg^{2+} ions. First, negatively charged carboxylic group of L-arginine binds to positively charged surface of the AuNRs. Then, at pH > 9.0, in the presence of Hg^{2+} ions, the L-arginine/AuNRs assemble side-by-side, which leads to red to green color change.

Cs^+, Cu^{2+}, K^+, Li^+, Ni^{2+}, Pb^{2+}, and Zn^{2+} were added into the L-arginine/AuNRs solution in the presence of 1 mM of Hg^{2+}.

Results and Discussions

Experimental optimization and proposed mechanism

Sensing strategy. The color of the L-arginine/AuNRs solution (Figure 2a) changed from red, which indicates the presence of AuNRs in the solution, to green with the addition of Hg^{2+} (1 mM). When the same experiments were performed using AuNRs without L-arginine functionalization, the solution color remained red with or without the addition of 1 mM of Hg^{2+}. Hence, the L-arginine functionalization of AuNRs is essential to produce color change and visible detection of Hg^{2+}. This color change occurs and becomes visible to the bare eye within 5 min of Hg^{2+} addition.

Generally, color change in solutions containing AuNPs occurs due to the shift in the plasmon band. Typically AuNRs exhibit 2 plasmon bands (Figure 2b). The more prominent peak in the NIR region corresponds to the longitudinal plasmon band, while the smaller peak around 500 nm is associated with the transverse plasmon band (Fang and others 2012). After Hg^{2+} addition there is a blue shift, that is, shift toward shorter wavelengths, in both the plasmon bands; however, the shift in the longitudinal plasmon band is more substantial along with significant decrease in signal intensity compared to that of the transverse plasmon band (Figure 2b). This suggests that, as expected, the longitudinal plasmon band is more sensitive to changes in the dielectric properties of the surrounding environment (Wang and others 2010).

This blue shift with decrease in amplitude of longitudinal surface plasmon peak might result from the modest side-by-side assembly of AuNRs (Wang and others 2010). TEM images of the L-arginine/AuNRs show that the AuNRs were well-dispersed within the solution before adding Hg^{2+} (Figure 2c); however, after Hg^{2+} addition, the AuNRs seemed to assemble along their longitudinal axis to some extent (Figure 2d). Side-by-side assembled structure is considered responsible for producing a blue shift of the longitudinal surface plasmon peak and concomitant color change (Xu and others 2011).

Effect of pH. Under the same experimental conditions, the system color change is dependent on the solution pH (Figure 3a). Over the tested pH range of 2.77 to 11.96, the color change occurs only when pH is higher than 9.0. This is due to the effect of pH on L-arginine. Figure 3b shows the structure of L-arginine, which has 3 p*K*a values: $pKa_1 = 2.02$ (α-carboxylic acid), $pKa_2 = 9.0$ (amine group), and $pKa_3 = 12.48$ (side chain group of amino acid) (Kumler and Eiler 1943). As can be seen from Figure 3c, when pH value was higher than 9.0 (pKa_2), the color started to change in the presence of Hg^{2+}. At this pH, both the carboxylic acid and amine groups of L-arginine are deprotonated (Figure 3c), which might become a bridge between Hg^{2+} and AuNRs in the sensing system.

During the synthesis of AuNRs, CTAB, a well-known cationic surfactant, forms a positively charged CTAB bilayer on the AuNRs (Gole and others 2004). Therefore, the attractive electrostatic interactions between the negatively charged carboxylic acid of L-arginine and positively charged CTAB bilayer on AuNRs might primarily be responsible for forming stable L-Arginine/AuNRs, while pH value is greater than 2.02 (pKa_1) (Gole and others 2004). When the pH value increase to more than 9, the deprotonated amine group of L-arginine would bind to Hg^{2+}, which is a possible reason for the AuNRs to assemble side-by-side. This suggested

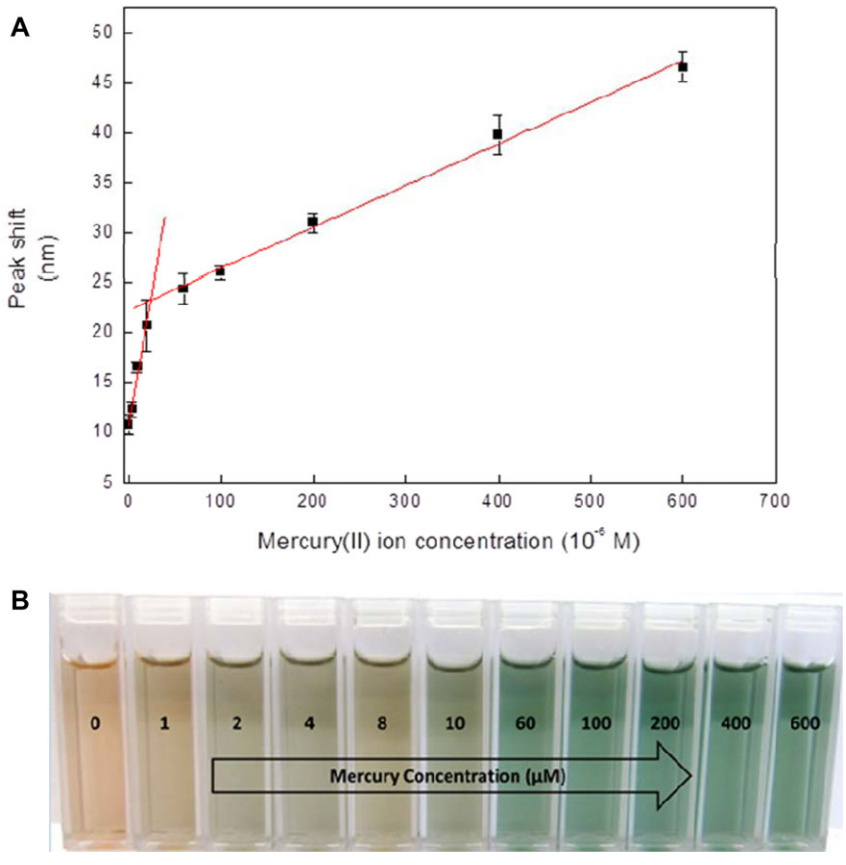

Figure 5–(a) Linear regressions of concentration of Hg^{2+} (in 2 ranges) compared with blue shift of the longitudinal band of L-arginine/AuNRs and (b) color of the L-arginine/AuNRs solution with 1 to 600 μM of Hg^{2+}.

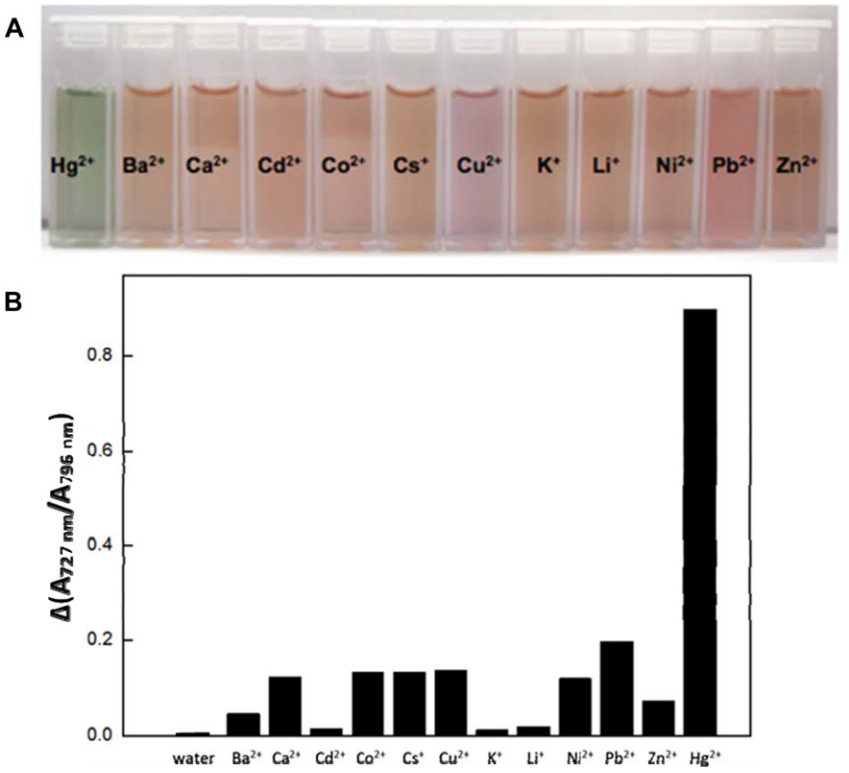

Figure 6–(a) Color of the L-arginine/AuNRs system with 1 mM Hg^{2+} and 10 mM of various metal ions. (b) The difference of $A_{727\ nm}/A_{796\ nm}$ of L-arginine/AuNRs system in the blank (water) and in the presence of various metal ions at pH 9.5.

AuNRs assembly mechanism is illustrated in Figure 4. We chose 9.5 as the optimal pH value for Hg^{2+} detection using our system.

Measuring Hg^{2+}

Calibration data for the determination of Hg^{2+} were obtained under an optimized set of experimental conditions. As seen in Figure 5a, the blue shift of the longitudinal band increased with increasing Hg^{2+} concentration. However, there appears to be 2 distinct ranges of Hg^{2+} concentration (C, μM) over which the peak shift increases fairly linearly: 1 to 20 μM and 20 to 600 μM. The corresponding linear regressions (each with $R^2 = 0.99$) are as follows:

$$1 \text{ to } 20\ \mu M\ Hg^{2+}\text{: Blue Shift (nm)} = 0.5307C + 10.464$$
$$20 \text{ to } 600\ \mu M\ Hg^{2+}\text{: Blue Shift (nm)} = 0.0416C + 22.223.$$

The LOD for Hg^{2+}, at a signal-to-noise ratio of 3, is calculated at 5 nM (MacNaught 2000). Figure 5b shows that in the presence of Hg^{2+}, the solution color changes from red to green, with the intensity of color change becoming deeper with increasing Hg^{2+} concentration.

Selectivity test

The selectivity of Hg^{2+} detection of our sensor in the presence of several other metal ions (Ba^{2+}, Ca^{2+}, Cd^{2+}, Co^{2+}, Cs^{+}, Cu^{2+}, K^{+}, Li^{+}, Ni^{2+}, Pb^{2+}, and Zn^{2+}) at 10 times the concentration of Hg^{2+} was very good. As shown in Figure 6a, the red-to-green color change occurred only for Hg^{2+}. The ratio of absorbance values at 727 nm and 796 nm, which are wavelengths of the longitudinal bands before and after the blue shift after adding Hg^{2+}, was used to determine the selectivity of Hg^{2+}. Further, to reduce the influence of other factors, the 727 nm/796 nm absorbance ratio value of blank (that is, water) was subtracted from that of the metal solutions (Figure 6b).

As can be seen from Figure 6, none of the metal ions tested interfered with the detection of Hg^{2+} even at 10 times the concentration. The small but measurable signals obtained with other metal ions (Figure 6b) are considered to be the result of changing dielectric properties of those metal ions at high concentrations, as they were tested at 10 times the concentration of Hg^{2+}. Further, the system color changed only in the presence of Hg^{2+} (Figure 6a). One possible explanation is that at pH > 9, the deprotonated amine group on L-arginine can bind only to Hg^{2+} (Palecek and others 1982; Delnomdedieu and others 1989; Safavi and Farjami 2011).

Conclusions

A simple, fast, and easy-to-use colorimetric assay for selective and sensitive determination of Hg^{2+} in water was developed based on surface plasmon resonance of L-arginine-functionalized AuNRs. By measuring the specific longitudinal plasmon band shift, which might relate to the side-by-side assembly of AuNRs, the L-agrinine/AuNRs system can be used to measure Hg^{2+} as low as 5 nM. The selectivity of Hg^{2+} detection is high as the system color change is largely unaffected by the presence of other metal ions (Ba^{2+}, Ca^{2+}, Cd^{2+}, Co^{2+}, Cs^{+}, Cu^{2+}, K^{+}, Li^{+}, Ni^{2+}, Pb^{2+}) even at 10 times the concentration of Hg^{2+}. This sensing method uses an environmentally friendly approach to functionalize AuNRs and provides a cost-effective way for detecting highly toxic Hg^{2+} in food and environmental samples.

Acknowledgments

This work was support by funding from the National Institute of Food and Agriculture, United States Department of Agriculture, under ID number WIS01644. The authors acknowledge use of instrumentation supported by the UW MRSEC (DMR-1121288) and the UW NSEC (DMR-0832760). The author Yi-Cheng

Wang acknowledge the support of Wisconsin Distinguished Graduate Fellowship and the IFT feeding tomorrow graduate scholarship.

References

Al-Mughairi S, Yesudhason P, Al-Busaidi M, Al-Waili A, Al-Rahbi WAK, Al-Mazrooei N, Al-Habsi SH. 2013. Concentration and exposure assessment of mercury in commercial fish and other seafood marketed in oman. J Food Sci 78(7):T1082–90.

Balarama Krishna MV, Castro J, Brewer TM, Marcus RK. 2007. Online mercury speciation through liquid chromatography with particle beam/electron ionization mass spectrometry detection. J Anal At Spectrom 22(3):283–91.

Chen G-H, Chen W-Y, Yen Y-C, Wang C-W, Chang H-T, Chen C-F. 2014. Detection of mercury(II) ions using colorimetric gold nanoparticles on paper-based analytical devices. Anal Chem 86(14):6843–49.

Clarkson TW, Magos L, Myers GJ. 2003. Human exposure to mercury: the three modern dilemmas. J Trace Elem Exp Med 16(4):321–43.

de Souza AC, de Carvalho AM. 2009. Metallic mercury embolism to the hand. N Engl J Med 360(5):507.

Delnomdedieu M, Boudou A, Desmazès J-P, Georgescauld D. 1989. Interaction of mercury chloride with the primary amine group of model membranes containing phosphatidylserine and phosphatidylethanolamine. Biochim Biophys Acta 986(2):191–9.

Fang, Y, Chang, W-S, Willingham B, Swanglap P, Dominguez-Medina S, Link S. 2012. Plasmon emission quantum yield of single gold nanorods as a function of aspect ratio. ACS Nano 6(8):7177–84.

FDA, U. S. F. a. D. A. 2014. Fish: What pregnant women and parents should know. Available from: http://www.fda.gov. Accessed 2014 August 06.

Gole A, Orendorff CJ, Murphy CJ. 2004. Immobilization of gold nanorods onto acid-terminated self-assembled monolayers via electrostatic interactions. Langmuir 20(17):7117–22.

Greenfield BK, Melwani AR, Allen RM, Slotton DG, Ayers SM, Harrold KH, Ridolfi K, Jahn A, Grenier JL, Sandheinrich MB. 2013. Seasonal and annual trends in forage fish mercury concentrations, San Francisco Bay. Sci Total Environ 444:591–601.

Guo Y, Wang Z, Qu W, Shao H, Jiang X. 2011. Colorimetric detection of mercury, lead and copper ions simultaneously using protein-functionalized gold nanoparticles. Biosens Bioelectron 26(10):4064–9.

Hsu IH, Hsu T-C, Sun Y-C. 2011. Gold-nanoparticle-based graphite furnace atomic absorption spectrometry amplification and magnetic separation method for sensitive detection of mercuric ions. Biosens Bioelectron 26(11):4605–9.

Hutter E, Maysinger D. 2013. Gold-nanoparticle-based biosensors for detection of enzyme activity. Trends Pharmacol Sci 34(9):497–507.

Jana NR, Gearheart L, Murphy CJ. 2001. Wet chemical synthesis of high aspect ratio cylindrical gold nanorods. J Phys Chem B 105(19):4065–7.

Jans H, Huo Q. 2012. Gold nanoparticle-enabled biological and chemical detection and analysis. Chem Soc Rev 41(7):2849–2866.

Kumler WD, Eiler JJ. 1943. The acid strength of mono and diesters of phosphoric acid. The n-alkyl esters from methyl to butyl, the esters of biological importance, and the natural guanidine phosphoric acids. J Am Chem Soc 65(12):2355–61.

Leopold K, Foulkes M, Worsfold P. 2010. Methods for the determination and speciation of mercury in natural waters—a review. Anal Chim Acta 663(2):127–38.

Li M, Wang Q, Shi X, Hornak LA, Wu N. 2011. Detection of mercury(II) by quantum Dot/DNA/Gold nanoparticle ensemble based nanosensor via nanometal surface energy transfer. Anal Chem 83(18):7061–5.

Lim S, Koo OK, You YS, Lee YE, Kim MS, Chang PS, Kang DH, Yu JH, Choi YJ, Gunasekaran S. 2012. Enhancing nanoparticle-based visible detection by controlling the extent of aggregation. Sci Rep 2, Article No. 456.

Lin Y-W, Huang C-C, Chang H-T. 2011. Gold nanoparticle probes for the detection of mercury, lead and copper ions. Analyst 136(5):863–71.

Liu X, Tang Y, Wang L, Zhang J, Song S, Fan C, Wang S. 2007. Optical detection of mercury(II) in aqueous solutions by using conjugated polymers and label-free oligonucleotides. Adv Mater 19(11):1471–4.

MacNaught AD. 2000. IUPAC compendium of chemical terminology. Research Triangle Park, N.C.: IUPAC.

Male YT, Reichelt-Brushett AJ, Pocock M, Nanlohy A. 2013. Recent mercury contamination from artisanal gold mining on Buru Island, Indonesia—potential future risks to environmental health and food safety. Mar Pollut Bull 77(1–2):428–33.

Mamdani H, Vettese TE. 2013. Pulmonary emboli caused by mercury. N Engl J Med 369(21):2031.

Mansour SA. 2014. Heavy metals of special concern to human health and environment. In: Practical food safety (Eds. R Bhat and VM Gomez-Lopez). John Wiley & Sons, Ltd, Chichester, West Sussex, UK. p 213–33.

Mutter J, Curth A, Naumann J, Deth R, Walach H. 2010. Does inorganic mercury play a role in alzheimer's disease? A systematic review and an integrated molecular mechanism. J Alzheimers Dis 22(2):357–74.

Nolan EM, Lippard SJ. 2008. Tools and tactics for the optical detection of mercuric ion. Chem Rev 108(9):3443–80.

Orendorff CJ, Murphy CJ. 2006. Quantitation of metal content in the silver-assisted growth of gold nanorods. J Phys Chem B 110(9):3990–4.

Palecek E, Osteryoung J, Osteryoung RA. 1982. Interactions of methylated adenine derivatives with the mercury electrode. Anal Chem 54(8):1389–94.

Placido T, Aragay G, Pons J, Comparelli R, Curri ML, Merkoçi A. 2013. Ion-directed assembly of gold nanorods: a strategy for mercury detection. ACS Appl Mater Interfaces 5(3):1084–92.

Qu Y, Zhang X, Wu Y, Li F, Hua J. 2014. Fluorescent conjugated polymers based on thiocarbonyl quinacridone for sensing mercury ion and bioimaging. Polym Chem 5(10):3396–403.

Safavi A, Farjami E. 2011. Construction of a carbon nanocomposite electrode based on amino acids functionalized gold nanoparticles for trace electrochemical detection of mercury. Anal Chim Acta 688(1):43–8.

Schober SE, Sinks TH, Jones RL, Bolger PM, McDowell M, Osterloh J, Garrett ES, Canady RA, Dillon CF, Sun Y, Joseph CB, Mahaffey KR. 2003. Blood mercury levels in us children and women of childbearing age, 1999–2000. J Am Med Assoc 289(13):1667–4.

Selin NE. 2009. Global biogeochemical cycling of mercury: a review. Annu Rev Environ Resour 34(1):43–63.

Tao H, Lin Y, Yan J, Di J. 2014. A plasmonic mercury sensor based on silver–gold alloy nanoparticles electrodeposited on indium tin oxide glass. Electrochem Commun 40:75–9.

Tchounwou PB, Ayensu WK, Ninashvili N, Sutton D. 2003. Review: environmental exposure to mercury and its toxicopathologic implications for public health. Environ Toxicol 18(3):149–75.

Ugo P, Zampieri S, Moretto LM, Paolucci D. 2001. Determination of mercury in process and lagoon waters by inductively coupled plasma-mass spectrometric analysis after electrochemical preconcentration: comparison with anodic stripping at gold and polymer coated electrodes. Anal Chim Acta 434(2):291–300.

Vigderman L, Khanal BP, Zubarev, ER. 2012. Functional gold nanorods: synthesis, self-assembly, and sensing applications. Adv Mater 24(36):4811–41.

Wang Y-C, Lu L, Gunasekaran S. 2015. Gold nanoparticle-based thermal history indicator for monitoring low-temperature storage. Microchimica Acta. (DOI 10.1007/s00604-015-1451-6)

Wang Y-C, Gunasekaran S. 2012. Spectroscopic and microscopic investigation of gold nanoparticle nucleation and growth mechanisms using gelatin as a stabilizer. J Nanopart Res 14(10): 1–11.

Wang L, Zhu Y, Xu L, Chen W, Kuang H, Liu L, Agarwal A, Xu C, Kotov NA. 2010. Side-by-side and end-to-end gold nanorod assemblies for environmental toxin sensing. Angew Chem Intl Ed 49(32):5472–5.

Wei Y, Li B, Wang X, Duan Y. 2014. A nano-graphite-DNA hybrid sensor for magnified fluorescent detection of mercury(II) ions in aqueous solution. Analyst 139(7):1618–21.

Xu L, Kuang H, Wang L, Xu C. 2011. Gold nanorod ensembles as artificial molecules for applications in sensors. J Mater Chem 21(42):16759–82.

Xue X, Wang F, Liu X. 2008. One-step, room temperature, colorimetric detection of mercury (Hg2+) using DNA/nanoparticle conjugates. J Am Chem Soc 130(11):3244–5.

Yasri NG, Sundramoorthy AK, Chang W-J, Gunasekaran S. 2014. Highly selective mercury detection at partially oxidized graphene/poly(3,4-ethylenedioxythiophene): poly (styrenesulfonate) nanocomposite film-modified electrode. FrontiersinMaterials 1, Article 33.

Zhu Z., Su Y., Li J., Li D., Zhang J., Song S., Zhao Y., Li G., Fan C. 2009. Highly sensitive electrochemical sensor for mercury(II) ions by using a mercury-specific oligonucleotide probe and gold nanoparticle-based amplification. Anal Chem 81(18):7660–6.